Petukhin and Iwasaki
Earth, Planets and Space (2023) 75:69
https://doi.org/10.1186/s40623-023-01824-5

Earth, Planets and Space

FULL PAPER

Open Access

Validation of the Osaka basin velocity model by waveform simulation using sources inverted with reciprocal Green's functions

Anatoly Petukhin[1*] and Yoshinori Iwasaki[1]

Abstract

To advance the methodology for validating velocity models by waveform comparison, we estimated source parameters for small magnitude earthquakes that can be approximated by point sources. Instead of using published source models, we used the reciprocity method to calculate 3D Green's functions using the target velocity structure itself, and then inverted the earthquake sources. This method greatly reduces the calculations required compared to a full inversion of the source mechanism, depth, and source duration (risetime), making it possible to reproduce input ground motions in the target basin. Here, we validated the Japan Integrated Velocity Structure model of the Osaka basin using five earthquakes around the Osaka basin; these earthquakes allowed us to investigate the impact of the incident waves' propagation directions. We first estimated source parameters using records at control bedrock sites surrounding the Osaka basin to reproduce the input ground motions. Then, we conducted a 3D finite-difference simulation for sites within the basin. By mapping the distributions of misfit values for individual waveforms, peak ground velocities, and response spectra, we were able to identify areas in the basin that require additional tuning of the velocity model.

Keywords Osaka basin model, FDM waveform simulation, Reciprocity method, Velocity model validation

*Correspondence:
Anatoly Petukhin
anatolyp@geor.or.jp
Full list of author information is available at the end of the article

Graphical Abstract

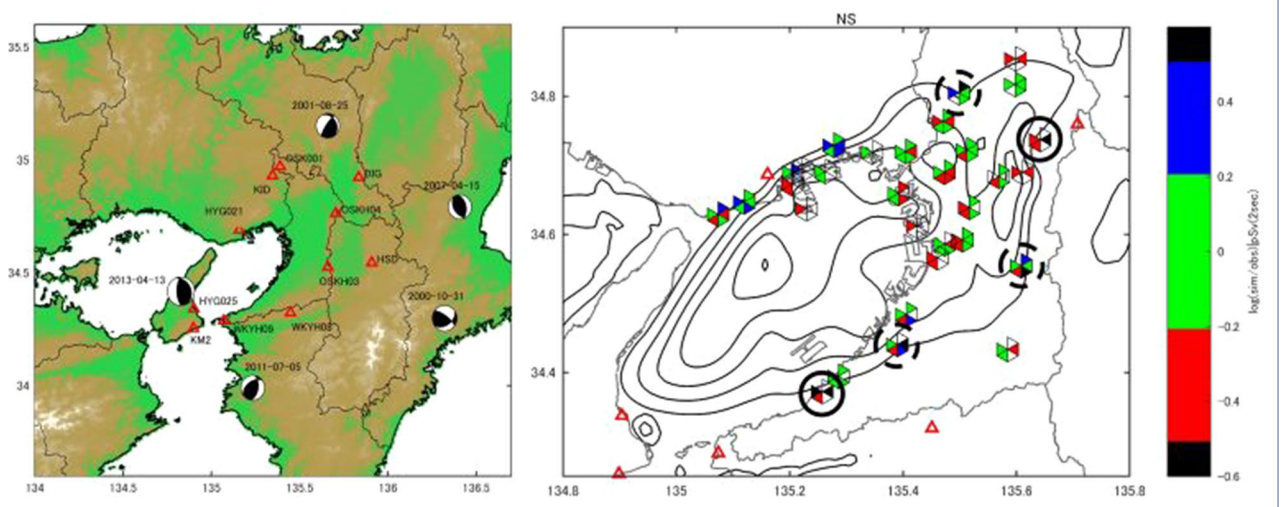

Introduction

The Osaka basin is a 2.5-km-deep sedimentary basin hosting the cities of Osaka and Kobe, as well as numerous structures vulnerable to long-period ground motions, such as skyscrapers, oil tanks, and long-span bridges. Thick sedimentary cover, such as in the Osaka basin, is known to enlarge ground motion amplitudes. Since the 1985 Michoacan earthquake, realistic heterogeneous source models and 3D velocity structures have been widely and successfully used to simulate and predict damaging long-period ground motions. Velocity structure models of the Osaka basin have been progressively developed as more data have become available (e.g., Iwasaki et al. 1994; Kagawa et al. 2004; Iwata et al. 2008). All these models have used spline interpolation for the bedrock depth (Koketsu and Higashi 1992) and a three-layer structure employing constant velocities within the layers and layer thicknesses proportional to the bedrock depth. Because they use just a few parameters, however, spline models are easily tuned; for example, Iwaki and Iwata (2011) used observed waveforms with periods > 3 s to improve waveform fit of the model of Iwata et al. (2008) by nonlinear inversion. Furthermore, Horikawa et al. (2003) and Sekiguchi et al. (2016) divided the spline interfaces with sheer planes to express steps along faults around and within the basin (Suehiro et al. 2003) and implemented velocity gradients within the structural layers. The increased detail in the model of Sekiguchi et al. (2016) is expected to better reproduce short-period waveforms compared to the spline model.

Further improvements in basin modeling require model validation to identify poorly modeled areas, followed by detailed and costly investigations of those areas. Validating velocity structure models by waveform simulation is straightforward and well suited to the problem of ground motion prediction. In many works this method is applied for validation of basin models, for example: San Bernardino basin, USA (Graves and Wald 2004); Santa Clara valley, USA (Hartzell et al. 2006); Los Angeles basin, USA (Lee and Chen 2016); Taipei basin, Taiwan (Lee et al. 2008); Mygdonian Basin, Greece (Maufroy et al. 2015); Southern California basins (Nweke et al. 2022); Po plain, Italy (Paolucci et al. 2015); Puget Sound basins, USA (Pitarka et al. 2004); Kanto basin, Japan (Takemura et al. 2015).

For this validation, it is necessary to estimate uncertain source parameters (e.g., source depth, source duration) for a medium-magnitude earthquake that is capable of generating long-period waves but that can still be approximated by a point source. Here, we used the reciprocity method (e.g., Eisner and Clayton 2001) to tune source parameters. This method greatly reduces the cost of 3D finite-difference (FDM) simulations and allows for more parameters to be tuned, including the focal mechanism. We used the open-source Japan Integrated Velocity Structure model (JIVSM; Koketsu et al. 2012) that includes the Osaka basin model developed by Kagawa et al. (2004). We chose five target events around the basin and first estimated source parameters (depth, source duration, and mechanism correction) using records at bedrock sites. Then, we developed a 3D FDM simulation for sites within the basin.

Source tuning

To estimate site amplification effects, the ratio of amplitude spectra at sedimentary and nearby bedrock sites is often used, or spectral inversion is used to determine source–path–site effects if nearby bedrock sites are unavailable (e.g., Andrews 1986; Iwata and Irikura 1988). For modeling of waveforms, bedrock site approach was modified by Wen and Helmberger (1997). They propose using transfer function that can be calculated numerically in case of 3D basins (e.g., Yoshida 2011). In this approach, ground motions at a bedrock site are used as the motion input at a nearby sedimentary site. However, sedimentary basins have the additional complexity that they are affected by the basin-edge generation of long-period waves as well as wave amplification, reflection, and interference (e.g., Kagawa et al. 1992; Frankel 1994; Graves et al. 1998; Ayoubi et al. 2021, and references therein). In such cases, instead of ground motions at a single site, it is necessary to use the entire wavefield simulated for an earthquake outside the basin. The source model of the earthquake should be tuned to reproduce observed waveforms at bedrock sites located in front of the target basin (control points). Simulated input wavefield along segments between the control points are also assumed to reproduce wavefield from the natural earthquake source.

We note that observed waveforms at bedrock sites on the opposite side of the basin from the epicenter are strongly contaminated by basin waves, which produce delayed trailing waves that degrade the pulse-like characteristic expected at bedrock sites (e.g., Ewald et al. 2006, their Fig. 3). Therefore, we exclusively used control sites between the basin and the epicenter for source tuning.

Most basins have complex shapes; the Osaka basin is elliptical, with steep edges on its northwestern and eastern sides and flat edges on its southern side (Figs. 1, 2). In this basin, therefore, the effects of basin-wave generation, reflection, and interference depend on the azimuth of the incoming waves (e.g., Kagawa et al. 1992). For this reason, to validate the Osaka basin model, we used five medium-magnitude earthquakes with epicenters to the north, east, southeast, south, and west of the basin (see Fig. 1 and Table 1 for earthquake locations and parameters).

Published source parameters require tuning because available velocity structure models and the Green's functions (GFs) used to estimate the source parameters have uncertainties that increase as the period of the target wave decreases. For example, the centroid-moment-tensor (CMT) solutions from two major Japanese agencies, F-net and JMA, differ because the agencies use different periods for their waveform inversions (Table 1). Thus, to avoid the effects of these uncertainties, long-period waves are commonly used to obtain CMT solutions (e.g., 20–30 s for F-net solutions; Aoi et al. 2020).

However, the objective of this study is to fit the short-period waveforms (as short as 2 s) that impact large-scale engineering structures. By careful tuning of the source parameters using waveform fit at short periods, effect of uncertainties of velocity model can be reduced. This procedure is equivalent to hypocenter relocation in seismic tomography, but uses the full waveform and the full set of source parameters. We used a nonlinear simplex search (SS) method (Lagarias et al. 1998) based on the initial source parameters estimated by F-net: source coordinates and depth, seismic moment, strike, dip, and rake. Target periods of the waveform misfit are 2–10 s.

We assumed symmetric bell functions for the time functions of the point sources. Bell functions require only one parameter, source duration *Ts*. To calculate waveforms over a large variety of source durations, we applied the spectral correction approach of Petukhin et al. (2017a). In the first step of the reciprocity method, we calculated GFs using bell functions and a dummy source duration value Ts^*. To calculate waveforms for the target source durations, which vary during the source inversion, we calculated the Fourier spectrum of each waveform for Ts^* and then converted it to the Fourier spectrum for the target *Ts* value using the equation:

$$WS(f) = WS^*(f) \cdot \frac{S(f|Ts)}{S(f|Ts*)}, \tag{1}$$

where $WS(f)$ is the spectrum of the target waveform, $WS^*(f)$ is the spectrum of the waveform for the dummy source duration, and $S(f \mid Ts^*)$ and $S(f \mid Ts)$ are the spectra of the source bell functions for the dummy and target source durations, respectively. Then, we performed an inverse Fourier transform to calculate the target waveform.

The initial models used for source tuning were F-net CMT solutions (Table 2). Initial source duration values were estimated from the velocity pulse width at the bedrock site nearest the source when available, or calculated as:

$$Ts = 0.5W/Vr, \tag{2}$$

where W is rupture width, and $Vr = 2.4$ km/s is the rupture velocity. For the 13 April 2013 earthquake, we used the model of Asano et al. (2016), in which the depth and source duration values were estimated by a grid search to fit the waveforms at the site nearest the source.

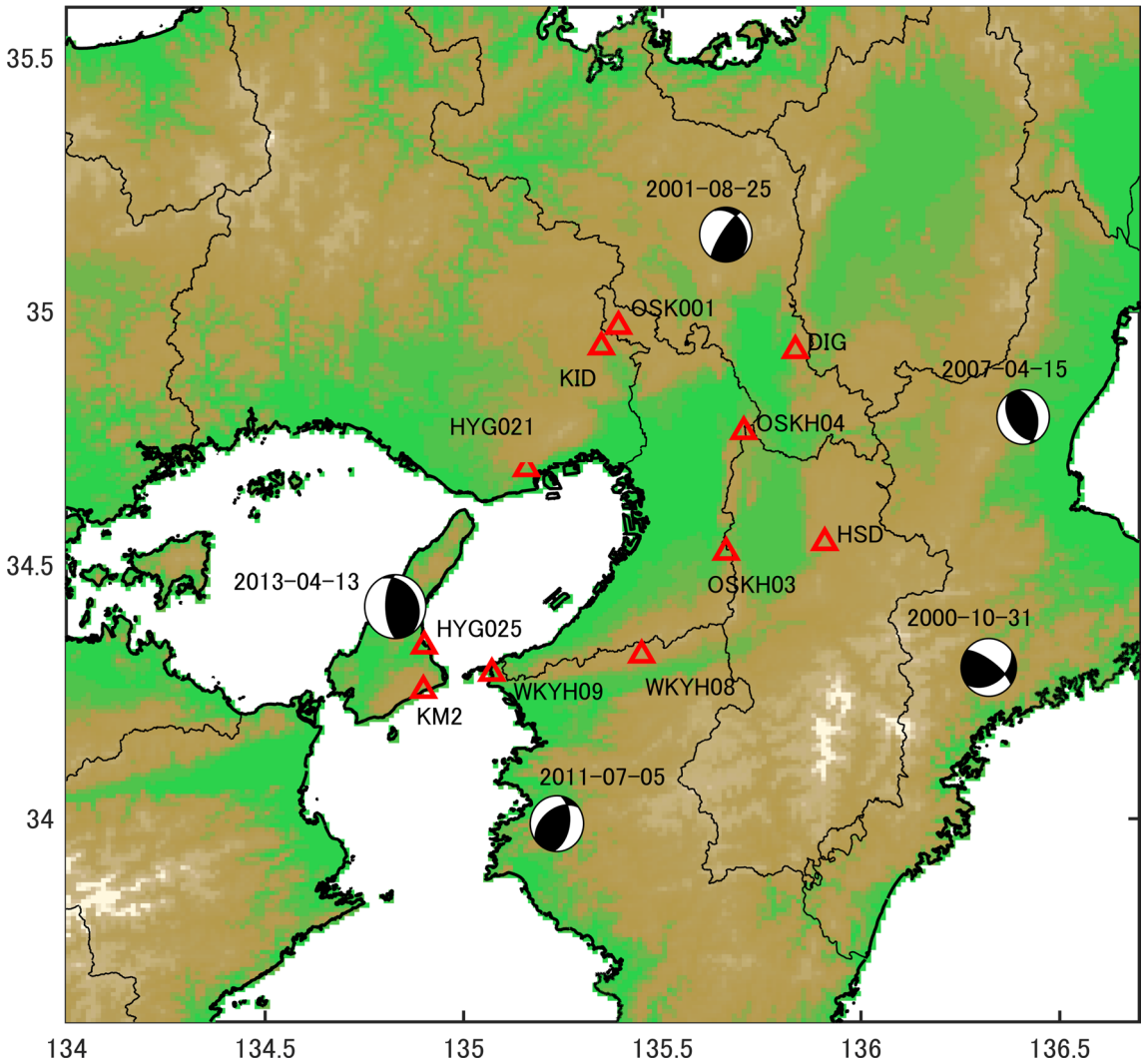

Fig. 1 Locations of target earthquakes ('beachball' symbols indicate the epicenter and focal mechanism) and bedrock control sites (triangles) used to tune the initial F-net solutions. The Osaka basin is in the center of map

Methodology of the simplex search

The SS method is a derivative-free method developed by Lagarias et al. (1998); implemented in Matlab and ready to use) that allows us to stably search for the minimum of the target function. The SS method requires an initial model, in the vicinity of which it searches for a minimum of the target function. In this way, we could identify models that both fit the waveforms and conformed to the realistic F-net solutions.

The waveform misfit (WM) adopted in the SS search is defined as:

$$\mathrm{WM} = \frac{\int_0^{t_\mathrm{d}} (V_{sim}(t) - V_{obs}(t))^2 dt}{\sqrt{\int_0^{t_\mathrm{d}} V_{sim}(t)^2 dt \cdot \int_0^{t_\mathrm{d}} V_{obs}(t)^2 dt}}, \tag{3}$$

where $V_{\mathrm{obs}}(t)$ and $V_{\mathrm{sim}}(t)$ are the observed and simulated velocity waveforms, respectively, and t_d the waveform duration. Before the misfit calculation, waveforms were adjusted to the common P-wave arrival time t_p, which was picked automatically and manually for the simulated and observed waveforms, respectively. For simulated waveforms, we used amplitude type t_p picker having threshold 1e−9 m/s. Considering that simulated waveform has zero amplitude before P-wave, this simple method works well.

The effectiveness of the SS method depends on the proximity of the initial model to the global minimum of the misfit function: that is, the search will identify the nearest minimum, be it a local or global minimum. For oscillating seismic waveforms, the WM will have many

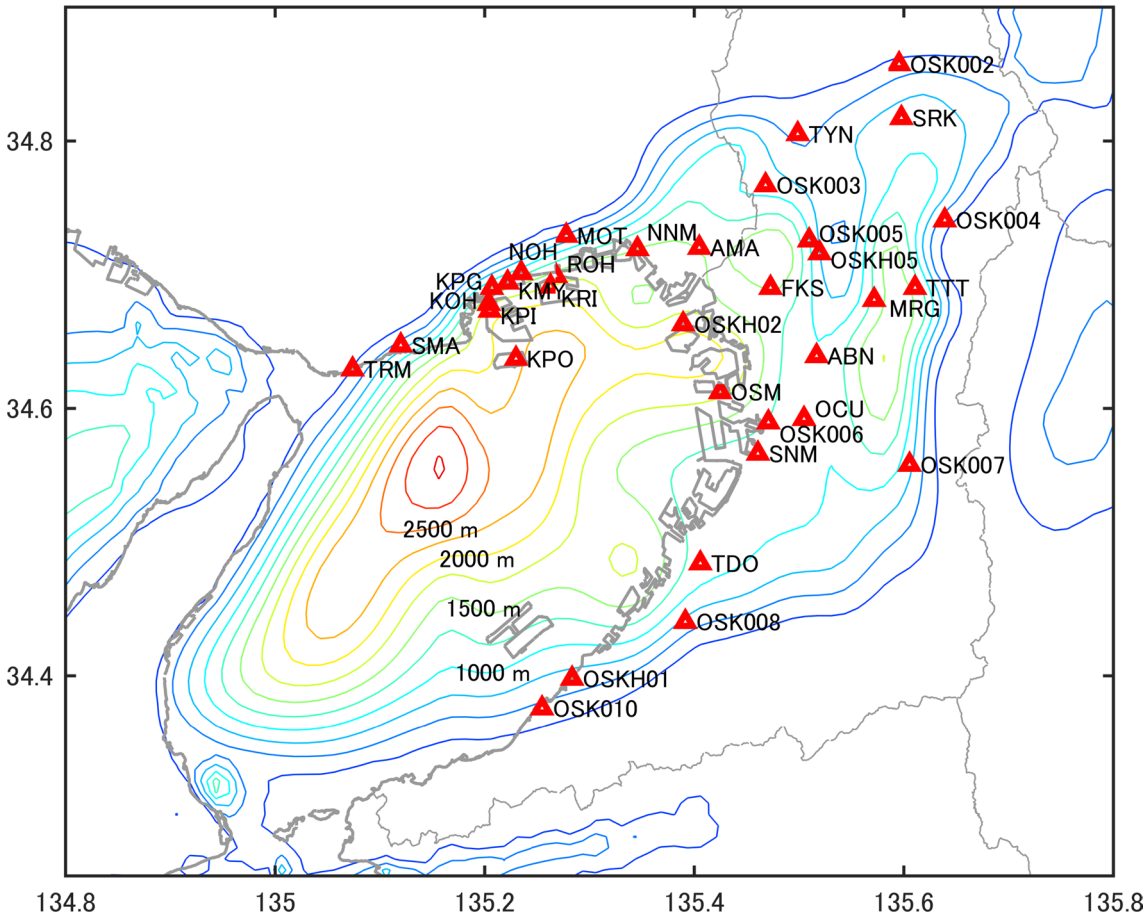

Fig. 2 Depth to bedrock in the Osaka basin (contour interval, 250 m). Basin sites used in our model validation are indicated by triangles

Table 1 Comparison of F-net and JMA CMT solutions for three of the earthquakes used as sources in our validation

Date	Ref	Lat	Lon	*H* (km)	*Mo* (Nm)	Strike	Dip	Rake
2001-08-25 M5.4	F-net	35.1472	135.6608	5.0	2.38e16	214	78	113
	JMA	35.0350	135.6400	10.0	3.58e16	353	18	71
2011-07-05 M5.5	F-net	33.9905	135.2342	8.0	3.35e16	9	52	59
	JMA	34.0150	135.2300	12.0	3.61e16	15	51	68
2013-04-13 M6.3	F-net	34.4188	134.8290	11.0	5.47e17	179	65	102
	JMA	34.4033	134.8300	17.0	7.00e17	175	60	95

minima and maxima, depending on the waveform shift. It is thus necessary for the initial model to be in the vicinity of the global minimum of the WM in parameter space. As the minimum waveform period $T_{\min}$ decreases, the number of minima of the WM increases, decreasing the probability that the initial model is in the vicinity of the global minimum. To guide the search process toward identifying the global minimum for short target periods ($T_{\min}=2$ s), we applied the following procedure.

Table 2 Tuned source parameters of the target earthquakes

Date	Ref	Lat	Lon	*H* (km)	*Ts* (s)	*Mo* (Nm)	Strike	Dip	Rake
2000-10-31 M5.7	F-net	34.2808	136.3485	38.0	1.1	1.70e17	306	72	130
	Tuned	34.2547	136.4094	31.8	0.88	1.52e17	300.3	95.2	142.3
2001-08-25 M5.4	F-net	35.1472	135.6608	5.0	1.3	2.38e16	214	78	113
	Tuned	34.9965	135.6887	5.0	1.64	3.38e16	379.8	23.0	78.8
2007-04-15 M4.6	F-net	34.7912	136.4077	11.0	2.4	3.94e16	347	46	103
	Tuned	34.8138	136.3493	7.6	1.82	2.88e16	338.2	41.0	104.9
2011-07-05 M5.5	F-net	33.9905	135.2342	8.0	0.5	3.35e16	9	52	59
	Tuned	34.0670	135.2626	6.4	1.63	3.11e16	6.6	58.5	79.2
2013-04-13 M6.3	A2016	34.4188	134.8290	14.6	3.5	5.47e17	179	65	102

Initial F-net solutions are included for comparison. We used the model tuned by Asano et al. (2016) for the 13 April 2013 earthquake

Step 1: We applied the SS method to a long-period waveform with $T_{\min}=5$ s. This reduced the number of secondary minima, thus increasing the probability that the initial model was in the vicinity of the global minimum of the WM.

Step 2: We then repeated the SS twice, each time decreasing $T_{\min}$ by 1 s (i.e., once at $T_{\min}=4$ s, and again at $T_{\min}=3$ s) and using result of the previous search as the initial model.

Step 3: We performed a final SS at the target value $T_{\min}=2$ s.

This procedure allowed us to maintain the initial model in the vicinity of the global minimum at each step. The assumed tolerance of the model and the misfit was 0.01, which allowed us to finish the search in several hundred SS iterations.

Reciprocity method

The simulation approach, based on the scaled summation of pre-calculated GFs, is an effective way to calculate ground motions for many source models, which is necessary for nonlinear source tuning. To calculate long-period GFs, we used the 3D FDM method, which is accurate but time-consuming. For this reason, pre-calculating the GFs for all possible source locations and depths by forward 3D FDM became practically impossible. Therefore, to reduce the simulation time, we employed the reciprocity method, described in detail by Eisner and Clayton (2001) and Graves and Wald (2001), and adopted GF calculations used for source inversions (e.g., Matsushima and Kawase 2009) or probabilistic analyses of long-period ground motions (e.g., Petukhin et al. 2017a, b).

In the first step of the reciprocity method, we calculated the responses of the three point-forces applied at the target site in the x, y, and z directions. Then, in the second step, the waveforms at each grid pair of the FDM double-couple source (see Graves 1996) were combined to produce a moment tensor response at the site. It is necessary to run a number of simulations equal to 3 times the number of control sites to calculate the GFs for all source locations at all control sites. Although the first step requires a few days of time on a computer cluster, it can be run in advance and the results stored in memory. In contrast, the calculations in the second step are faster, requiring only an assumption of the focal mechanism; waveforms for hundreds of source models can be calculated in a few minutes on a desktop computer.

Source tuning results

We used the 2015 release of the JIVSM for 3D waveform simulations (Koketsu et al. 2012). The model consists of 23 constant-velocity layers, including crustal and subduction zone layers, that were previously validated and tuned around, but not within, the Osaka basin by waveform simulations (Petukhin et al. 2012). This model is thus ready to use for simulating ground motions. Parameters assigned within each layer are *Vp*, *Vs*, density, as well as frequency-independent attenuation quality factors *Qp* and *Qs*. In this study we assumed for simplicity that $Qp=Qs$. Within sedimentary layers JIVSM model assumes that $Qs=Vs/5$, where *Vs* is in m/s. Our calculation area was 133.5–136.7° E and 33.6–35.8° N, with boundaries approximately 100 km beyond the basin; most of the calculation area is shown in Fig. 1. The depth of the calculation volume was 60 km, well below the Moho. Reflections from the Moho reduce the effects of possible reflections from the bottom of the calculation

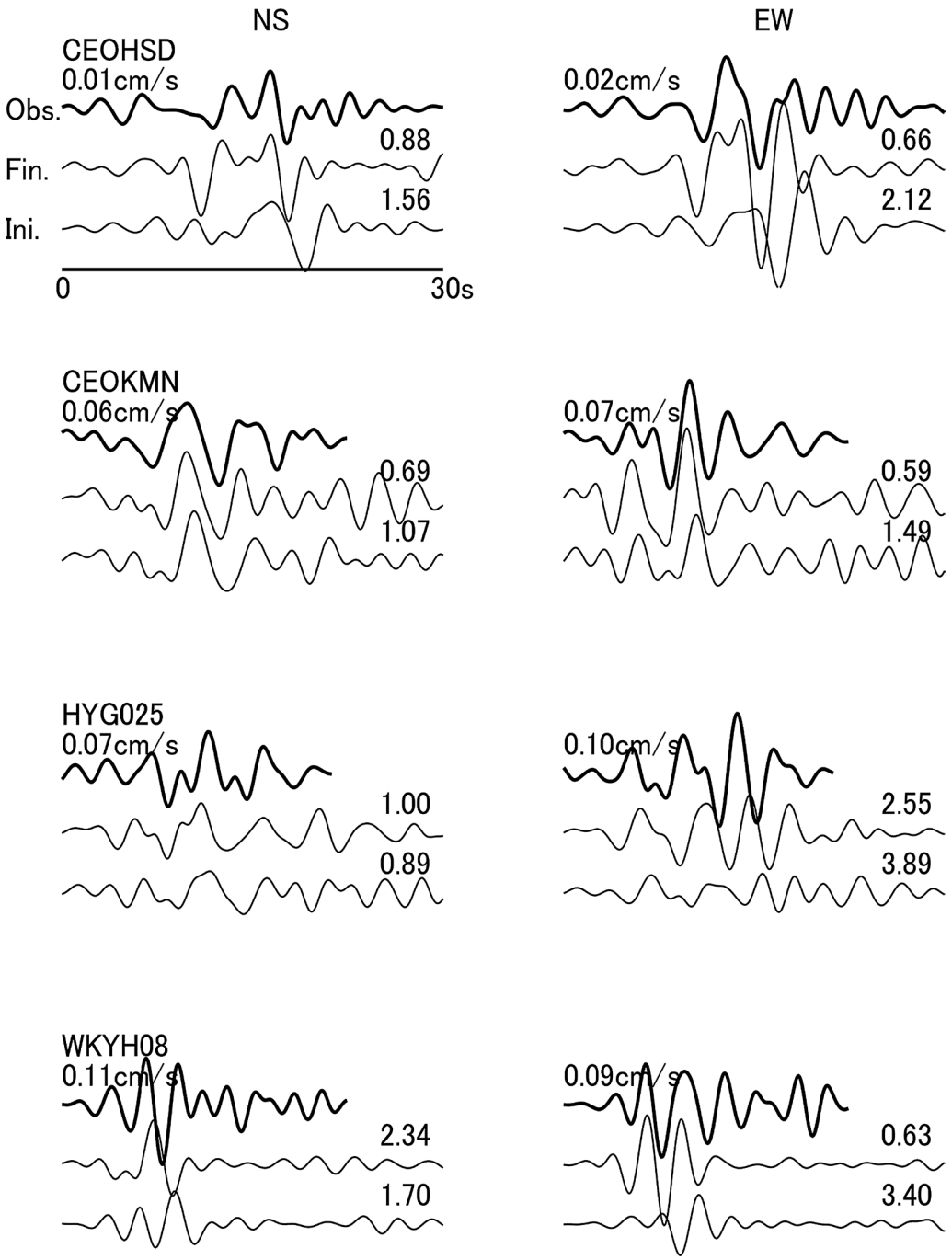

Fig. 3 Waveform fits for bedrock control sites outside the Osaka basin for the 5 July 2011 earthquake (fits for other earthquakes are shown in Additional file 1: Figs. S1–S4). Top, observed waveforms ('Obs.'); bottom, waveforms calculated for the initial F-net source ('Ini.'); center, waveforms calculated for the tuned source obtained herein ('Fin.'). Waveforms start at the P-wave arrival, waveform periods are 2–10 s, observed waveforms are labeled with their peak values, and calculated waveforms are labeled with their misfit values

volume. We used the staggered-grid method of Graves (1996). The FDM grid spacing was 280 m, allowing time steps 0.0085 s in the waveform simulations up to 2 s at the control sites. Within the basin, the grid spacing was refined to 140 m using a non-uniform grid (Pitarka 1999).

Our source tuning results are reported in Table 2. The tuned source locations and depths are compatible with the differences between the JMA hypocenters and the F-net CMT solutions. Except for the 25 August 2001 earthquake, the differences between the tuned focal mechanisms and the initial CMT solutions were minor and compatible with the differences between the F-net and JMA solutions. Because the source of the 13 April 2013 earthquake was just beneath the edge of the basin, we used the model previously tuned by Asano et al. (2016). An example of the improvement of the waveforms at bedrock sites is given for the 5 July 2011 earthquake (Fig. 3). In this example, our source tuning improved *WM* values at all target sites except HYG025, where only the E–W component was improved. The increased *WM* value for the N–S component at WKYH08 is due only to a waveform shift; the major pulse is better reproduced by the tuned source model than by the initial source model. The complete set of waveform comparisons is provided in Additional file 1. Overall, our tuning improved the WM values for 70% of the waveforms at the control sites.

Basin waveform simulation and validation results

The locations of the strong-motion stations used in our basin validation simulation are shown in Fig. 2. Osaka basin model comprises three sedimentary layers ($V_S = 0.35$, 0.6, and 1.0 km/s with increasing depth) with interfaces at 0.19 and 0.47 times the bedrock depth. These coefficients are subject for additional tuning by waveform modeling. For example, Iwaki and Iwata (2011) used values 0.12 and 0.41, respectively, while Guo et al. (2013) revised them to 0.08 and 0.39. Bedrock layers beneath the basin are from the JIVSM and have $V_S = 2.4$ and 3.2 km/s with increasing depth (for details, see Kagawa et al. 2004). The depth to bedrock is shown as contours in Fig. 2. For the 3D waveform simulations, we used the same FDM settings used for source tuning with a minimum simulated period of 2 s. Waveform comparisons for the 5 July 2011 earthquake are shown in Fig. 4; results for the other earthquakes are provided in Additional file 1. The distributions of *WM* values for the N–S component of each earthquake are mapped in Fig. 5. *WM* values are calculated with excluding later phases, i.e., for the 40-s segment of waveform, starting from t_P. To indicate the azimuthal dependence of the goodness-of-fit (lower *WM* values), *WM* values are plotted in segmented hexagons, with each segment roughly corresponding to the azimuth from which the incident waves propagated.

To facilitate our analysis, we classified the WM values as 'Very good' (< 1.0), 'Good' (1.0–2.0), 'Bad' (2.0–3.0), and 'Very bad' (> 3.0) (Fig. 6). We also calculated and classified the ratios of simulated to observed peak ground velocities (PGV) as 'Good' (1/1.5 to 1.5), 'Bad, overestimated' (1.5–3.0), 'Bad, underestimated' (1/3.0 to 1/1.5), and 'Very bad' (< 1/3.0 or > 3.0) (reported as log values in Fig. 7). Similarly, Figs. 8, 9, 10 and 11 show the ratios of simulated to observed response spectra (pseudo velocities, *pSv*) for wave periods of 2, 3, 5, and 7 s, respectively, classified based on the same ranges as the PGV ratios. Sites with especially bad fits are circled in Figs. 6, 7, 8, 9, 10 and 11; solid circles indicate sites with bad fits for multiple incident azimuths, dashed circles indicate sites with a bad fit for only one azimuth, and circle colors correspond to the misfits classification (black, 'Very Bad'; red, 'Bad' or 'Bad, underestimated'). We focus on underestimates because they are more likely to result in disaster than overestimates.

Analysis of Figs. 4, 5, 6, 7, 8, 9, 10 and 11 reveals that:

1. Simulated S-wave arrival times agree with the observations at most sites (Fig. 4), except those with unclear S-wave arrivals (e.g., MRG and OSK005).
2. Waveform fits for direct waves (~ 20 s after the S-wave arrivals in Fig. 4) are good at many sites in terms of amplitude and phase, except those near the edges of the basin (e.g., OSK004, OSK010, OSKH01, OSK008, ABN), for which amplitudes are largely underestimated in one or both components. Detailed explorations may be necessary around those sites.
3. Fitting later phases of basin waves is challenging. With few exceptions (N–S components at sites KRI and MRG, E–W component at site KPI), the later phases have different waveforms (Fig. 4). Nonetheless, the amplitudes of later simulated phases fit the observed amplitudes with errors of ± 50% at most of sites, which is acceptable. We note that the good fit of reflected and converted/interfered later phases, which appear ~ 40 s after S-arrival and later, depend on the accuracy of the modeling at the basin edges.
4. The distributions of the WM misfits and the PGV and *pSv* ratios show that most sites with poor fits

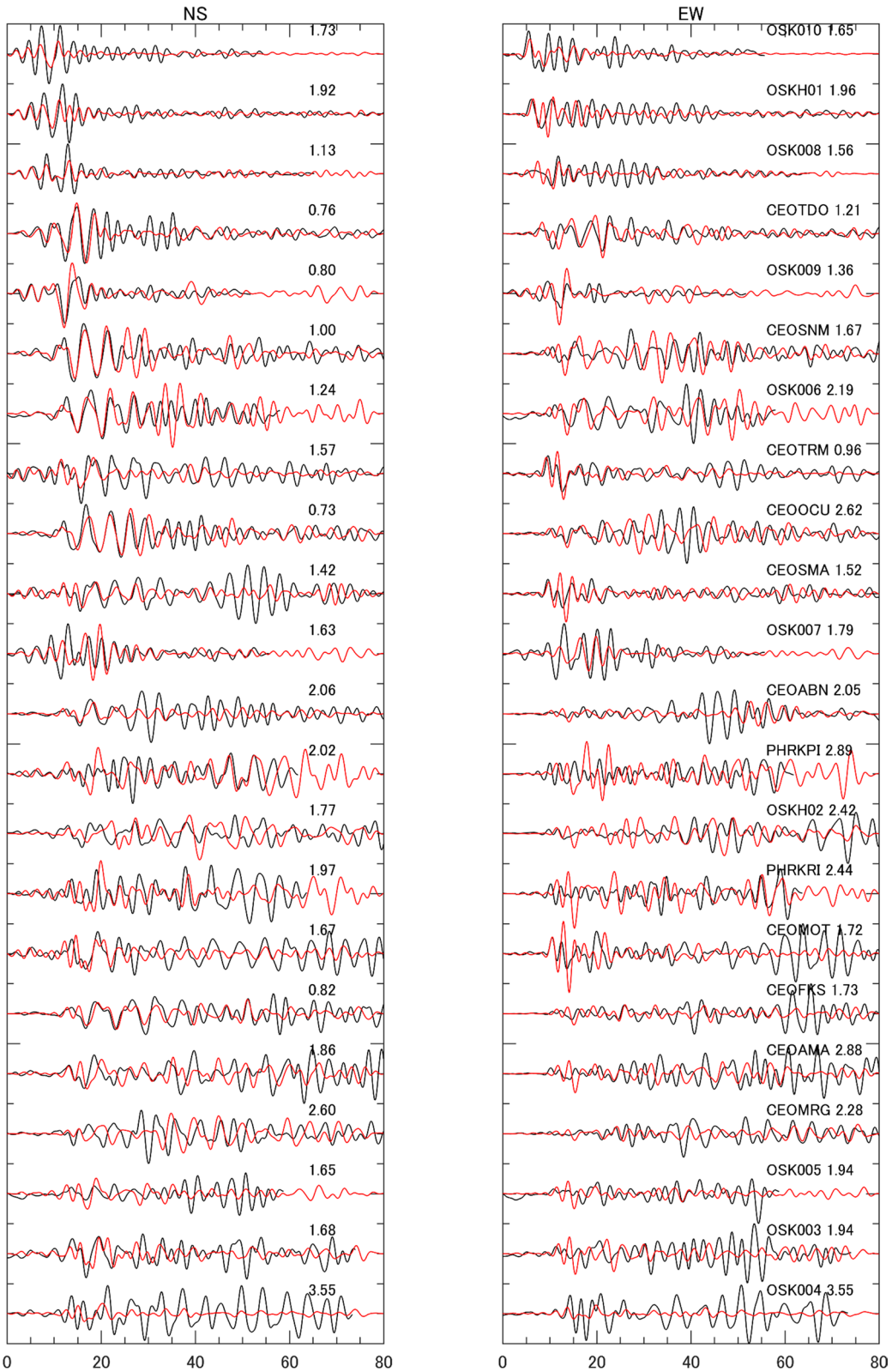

Fig. 4 Waveform fits for N–S (left) and E–W (right) components at basin sites for the 5 July 2011 earthquake (fits for other earthquakes are shown in Additional file 1: Figs. S5–S8). Black and red traces are observed and simulated waveforms, respectively. Waveforms start at the P-wave arrival, are normalized to unit amplitude, and are labeled with their misfit values

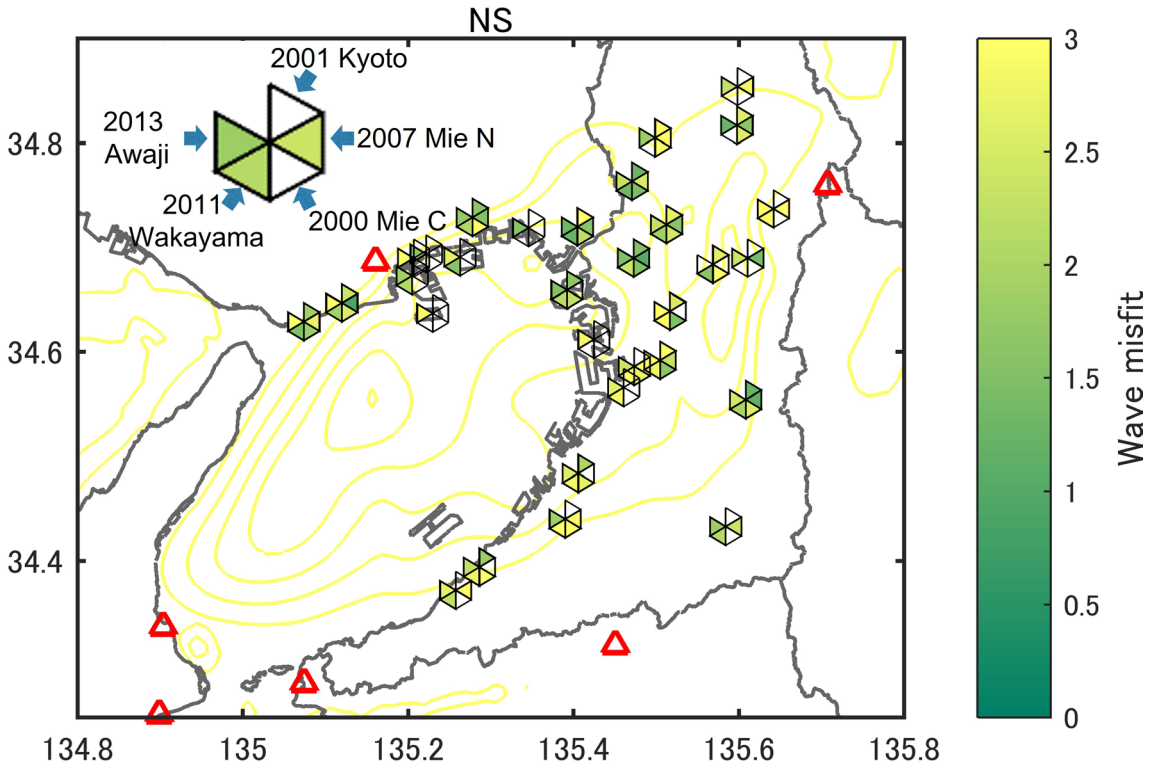

Fig. 5 The waveform misfit distribution for N–S components at basin sites. Symbols indicate the azimuthal direction of the earthquake hypocenters

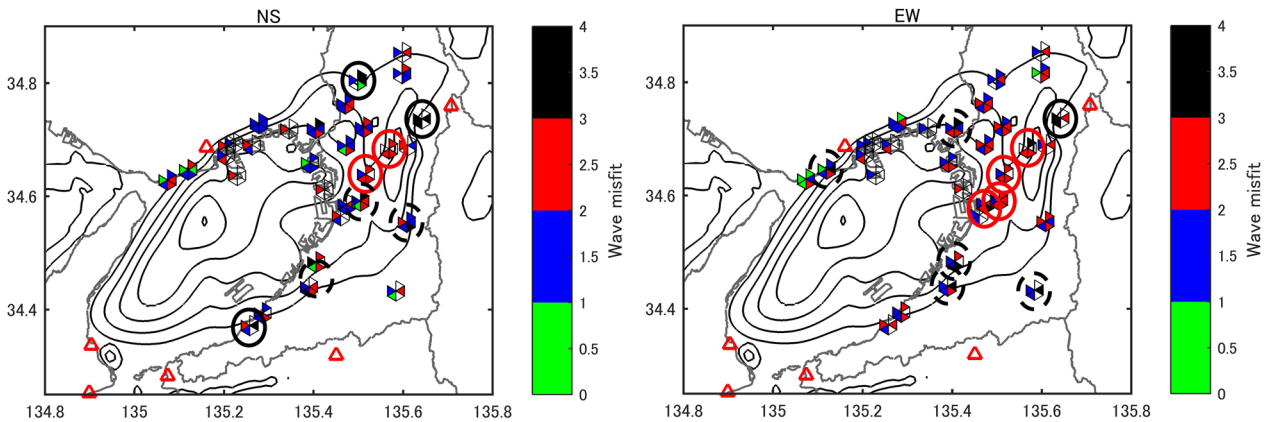

Fig. 6 Waveform misfits for the N–S (left) and E–W (right) components at basin sites, classified as very good (green), good (blue), bad (red), or very bad (black). Azimuthal symbols are as in Fig. 5. Dashed and solid circles indicate sites with particularly poor fits for a single or numerous azimuths, respectively

are near the basin edges, although there are also examples within the basin (e.g., sites FKS, ABN, and MRG). Asano et al. (2016) also reported large misfits for later phases at these sites during the 13 April 2013 earthquake using the basin model of Sekiguchi et al. (2016), especially for long periods of 6 s.

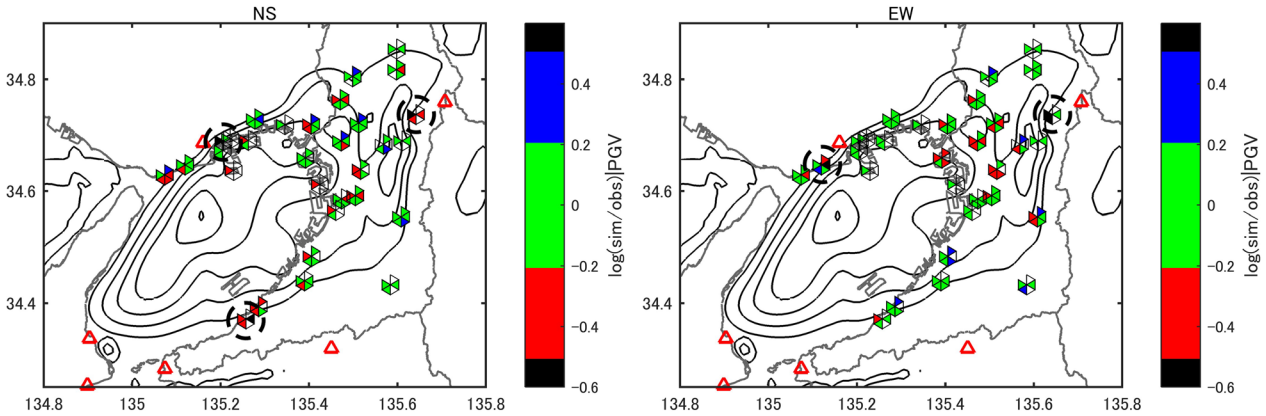

Fig. 7 The distribution of the ratios of simulated to observed peak ground velocities (PGVs, log scale) for the N–S (left) and E–W (right) components at basin sites. Azimuthal symbols are as in Fig. 5. PGV misfits are classified as good (green), bad and overestimated (blue), bad and underestimated (red), and very bad (black)

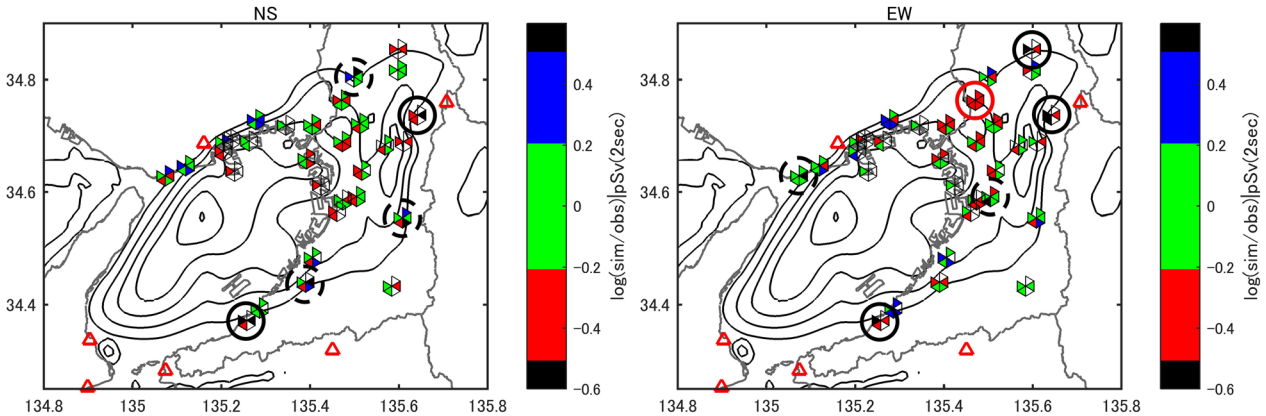

Fig. 8 The distribution of the ratios of simulated to observed response spectra *pSv* for a wave-period of 2 s for the N–S (left) and E–W (right) components at basin sites. Azimuthal symbols are as in Fig. 5. PSV misfits are classified as good (green), bad and overestimated (blue), bad and underestimated (red), and very bad (black)

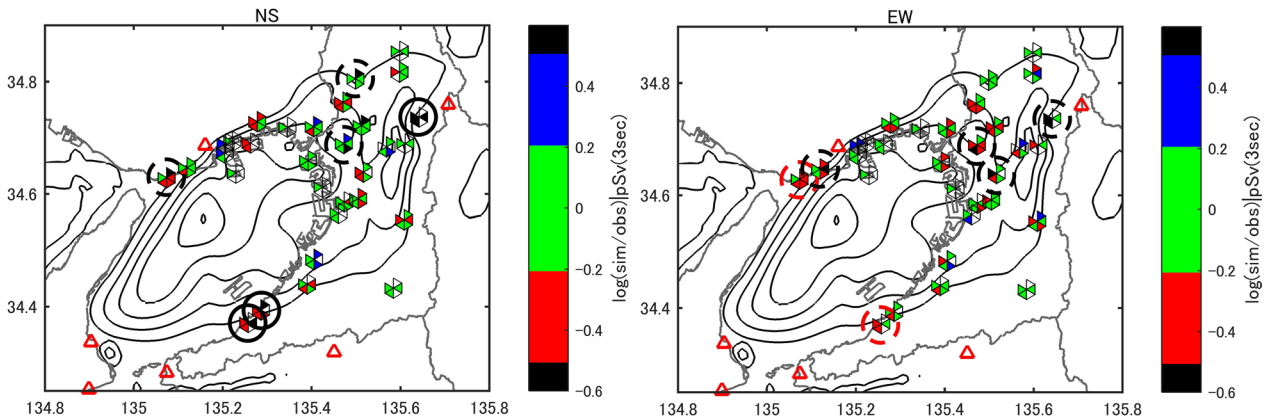

Fig. 9 The distribution of the ratios of simulated to observed response spectra *pSv* for a wave-period of 3 s for the N–S (left) and E–W (right) components at basin sites. Symbols and color scale are as in Fig. 8

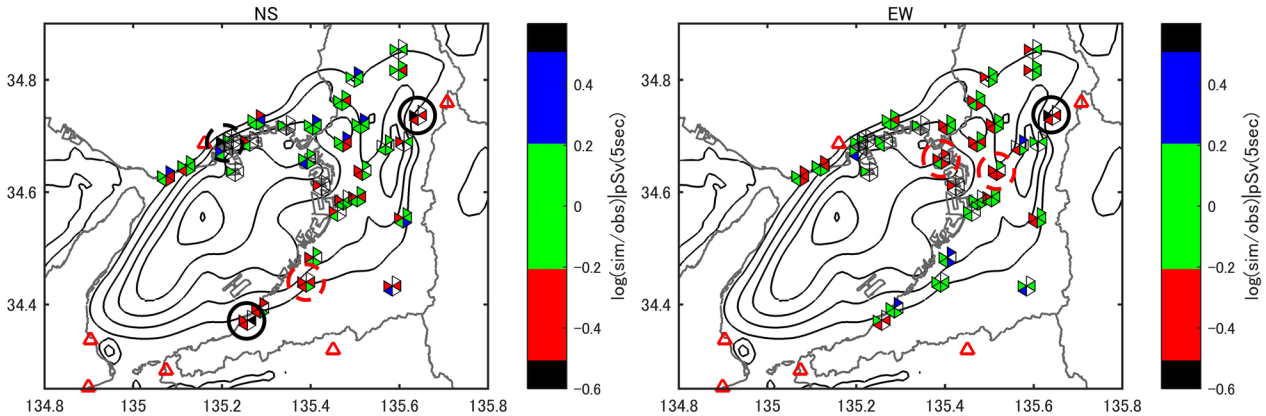

Fig. 10 The distribution of the ratios of simulated to observed response spectra *pSv* for a wave-period of 5 s for the N–S (left) and E–W (right) components at basin sites. Symbols and color scale are as in Fig. 8

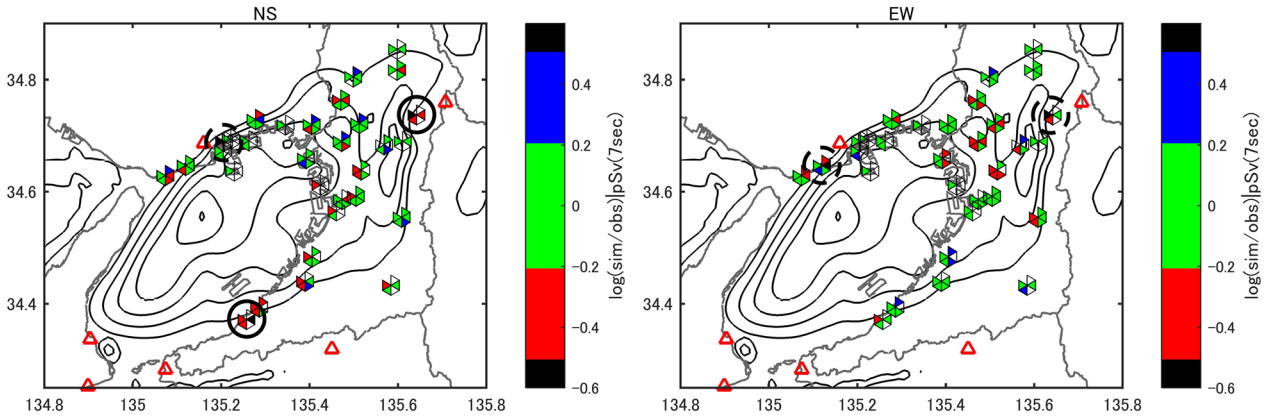

Fig. 11 The distribution of the ratios of simulated to observed response spectra *pSv* for a wave-period of 7 s for the N–S (left) and E–W (right) components at basin sites. Symbols and color scale are as in Fig. 8

5. Analysis of the misfits of the period-dependent parameter *pSv* indicates that misfits improve with increasing wave period. For example, the total number of azimuth sectors classified as 'Bad' or 'Bad, underestimated' in Figs. 8, 9, 10 and 11 decreases gradually from 42% at a period of 2 s to 30% at a period of 7 s. This is expected because uncertainties of velocity structure model decrease as the period of the target wave increases.

This analysis identifies sites in the Osaka basin that require detailed exploration and improvement.

Discussion

There are some issues with the method of basin model validation by waveform simulation for tuned sources. For example, the amplitudes of basin waveforms for the 31 October 2000 earthquake were systematically overestimated (Additional file 1: Fig. S5), probably because the source duration value used was too short ($Ts = 0.88$) for this M5.7 earthquake (Table 2). In addition to major effect of source duration to change frequency content of generated waves, there is an effect of waveform shift in time. For example, smaller source duration results in earlier arrival of waves. First effect is our target when we model waveforms. However, for calculation of WM value, second effect can be larger. In such cases, it may be

necessary to manually correct short source durations to larger values, which does not affect the waveform fits at bedrock sites.

The predominant period of ground motions is an important parameter from an engineering standpoint. Miyakoshi et al. (2013) used a 1D approximation to compute and map theoretical site responses to Love waves in the Osaka basin. However, a preliminary analysis of predominant ground motion periods from simulated waveforms considering 3D effects (Petukhin et al. 2017a) indicates that multiple spectral peaks exist. Depending on numerous factors (e.g., depth to bedrock, distance to the basin edge), some spectral peaks become dominant, making interpretations of predominant ground motion periods difficult; improving these interpretations should be the focus of future work.

We limited our analysis of the basin waveforms to the 80 s following the P-wave arrival. At most sites, the largest amplitude waves arrive during that window. However, in some cases, large amplitude phases can arrive later. For example, Asano et al. (2016) reported the arrival of a large amplitude phase at 100 s after the P-wave arrival during the 13 April 2013 earthquake, which is difficult to reproduce with existing basin models. Further basin modeling is thus necessary, and should focus on critical areas like the Osaka bay area in the southwest part of the Osaka basin, where the late phase reported by Asano et al. (2016) was generated or amplified. In this area particularly, new seabed observations may be necessary.

Our results indicate that most of the poorly reproduced sites are near basin edges. This result is probably due to oversmoothing cause by the spline interpolation. Validation using the model of Sekiguchi et al. (2016) should be prioritized because their model includes detailed information on steps in the velocity model due to faults surrounding the basin.

Finally, we should notice that accuracy of waveform fitting depends on the accuracy of FDM waveform simulation, in addition to the accuracy of velocity structure model. Specifically, smaller grid spacing increases waveform accuracy. Moczo et al. (2011) analyzed effect of grid spacing and found that with increasing Vp/Vs ratio necessary grid spacing should be decreased. JIVSM model in this study has $Vp/Vs=4.86$ in the shallowest layer. According to Moczo et al. (2011), this requires 8 grids per wavelength, i.e., 87.5 m for $T_{\min}=2$ s which is smaller than grid spacing 140 m (5 grids per wavelength) assumed in this study. To test effect of smaller grid spacing, waveforms in Fig. 4 additionally calculated with grid spacing 87.5 m. Results are compared in Appendix, Fig. 12. Although there is some waveform difference, we cannot conclude that smaller grid improves waveform fit: half of waveforms have improved *WM* value, while in another half *WM* value has degraded. Probable reason is that predominant periods inside Osaka basin are 3-to-7 s (e.g., Miyakoshi et al. 2013), which are larger than $T_{\min}=2$ s. From another side, smaller grid spacing is largely increasing computation cost largely; 6.5 times here. We will need to improve accuracy of waveform simulation in future work, as soon as getting improved velocity structures.

Conclusions

We applied the reciprocity method to tune the source models of medium-magnitude earthquakes around the Osaka basin. These source models were used to simulate 3D waveforms inside the basin, which we compared to waveforms observed at the same sites. Our comparison revealed that certain areas near the basin edges require detailed further exploration. We expect that future improvements to the basin model, especially near basin edges, will improve the waveform fit throughout the basin.

Appendix

In Fig. 12, we compare waveforms calculated for grid spacing 87.5 m according to recommendation of Moczo et al. (2011) with waveforms calculated in this study for grid spacing 140 m.

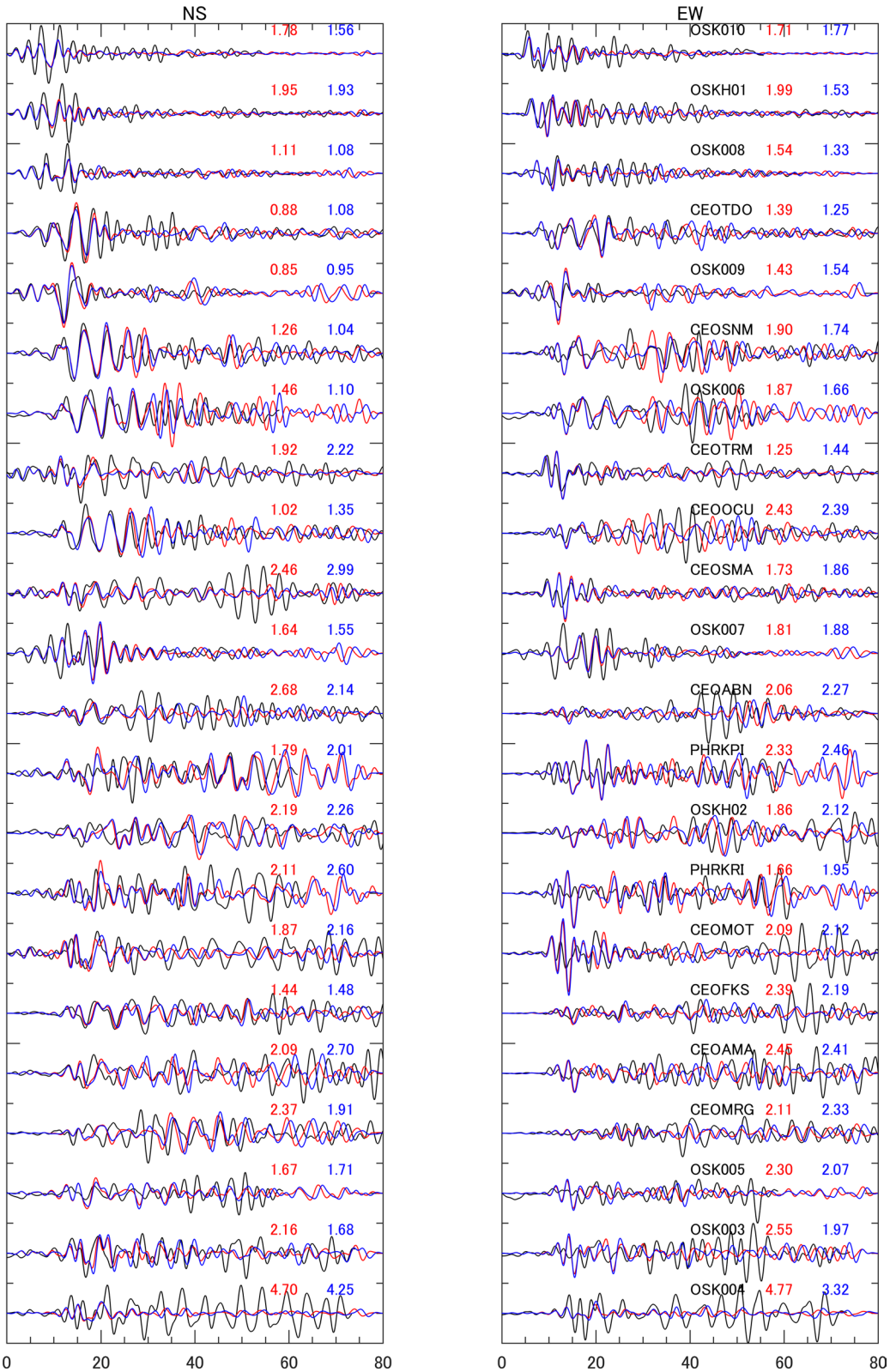

Fig. 12 Waveform fits for N–S (left) and E–W (right) components at basin sites for the 5 July 2011 earthquake. Black traces are observed waveforms. Red traces are waveforms simulated with grid spacing 140 m within the basin. Blue traces are waveforms simulated with grid spacing 87.5 m within the basin. Waveforms start at the P-wave arrival and are labeled with their misfit values colored, respectively

Supplementary Information

The online version contains supplementary material available at https://doi.org/10.1186/s40623-023-01824-5.

Additional file 1. Auxiliary material: Waveform comparison for all analyzed earthquakes.

Acknowledgements
This work was inspired by Asano et al. (2016). We used waveform data from the CEORKA, K-NET, Kik-net, and PARI networks, and CMT solutions from F-net and JMA. We are thankful to two anonymous reviewers and Associated Editor Fabrice Cotton for helpful comments that strongly improved manuscript.

Author contributions
AP performed the simulations and inversion analysis. AP wrote the initial draft of the manuscript through discussion with YI, who proposed the study. Both authors have proofread the draft. Both authors read and approved the final manuscript.

Declarations

Competing interests
The authors declare that they have no competing interests.

Author details
[1]Geo-Research Institute, Otemae 2-1-2, Chuo-ku, Osaka 540-0008, Japan.

Received: 28 September 2022 Accepted: 15 April 2023
Published online: 04 May 2023

References

Andrews DJ (1986) Objective determination of source parameters and similarity of earthquakes of different size. In: Boatwright J, Das S, Scholz CH (eds) Earthquake source mechanics, AGU monograph. doi:https://doi.org/10.1029/GM037.

Aoi S, Asano Y, Kunugi T, Kimura T, Uehira K, Takahashi N, Ueda H, Shiomi K, Matsumoto T, Fujiwara H (2020) MOWLAS: NIED observation network for earthquake, tsunami and volcano. Earth Planet Space 72:126. https://doi.org/10.1186/s40623-020-01250-x

Asano K, Sekiguchi H, Iwata T, Yoshimi M, Hayashida T, Saomoto H, Horikawa H (2016) Modelling of wave propagation and attenuation in the Osaka sedimentary basin, western Japan, during the 2013 Awaji Island earthquake. Geophys J Int 204:1678–1694. https://doi.org/10.1093/gji/ggv543

Ayoubi P, Mohammadi K, Asimaki D (2021) A systematic analysis of basin effects on surface ground motion. Soil Dyn Earthq Eng 141:106490. https://doi.org/10.1016/j.soildyn.2020.106490

Eisner L, Clayton RW (2001) A reciprocity method for multiple-source simulations. Bull Seism Soc Am 91:553–560. https://doi.org/10.1785/012000222

Ewald M, Igel H, Hinzen K-G, Scherbaum F (2006) Basin-related effects on ground motion for earthquake scenarios in the Lower Rhine Embayment. Geophys J Int 166:197–212. https://doi.org/10.1111/j.1365-246X.2006.02909.x

Frankel A (1994) Dense array recordings in the San Bernardino Valley of Landers-Big Bear aftershocks: basin surface waves, Moho reflections, and three-dimensional simulations. Bull Seism Soc Am 84:613–624. https://doi.org/10.1785/BSSA0840030613

Graves RW (1996) Simulating seismic wave propagation in 3D elastic media using staggered-grid finite differences. Bull Seism Soc Am 86:1091–1106. https://doi.org/10.1785/BSSA0860041091

Graves R, Wald D (2001) Resolution analysis of finite fault source inversion using 1D and 3D Green's functions. I strong motions. J Geophys Res 106:8767–8788

Graves RW, Wald DJ (2004) Observed and simulated ground motions in the San Bernardino Basin Region for the Hector Mine, California, Earthquake. Bull Seism Soc Am 94:131–146. https://doi.org/10.1785/0120030025

Graves RW, Pitarka A, Somerville PG (1998) Ground-motion amplification in the Santa Monica area: effects of shallow basin edge structure. Bull Seism Soc Am 88:1224–1242. https://doi.org/10.1785/BSSA0880051224

Guo Y, Koketsu K, Ohno T (2013) Analysis of the rupture process of the 1995 Kobe earthquake using a 3D velocity structure. Earth Planet Space 65:1581–1586. https://doi.org/10.5047/eps.2013.07.006

Hartzell S, Harmsen S, Williams RA, Carver D, Frankel A, Choy G, Liu P-C, Jachens RC, Brocher TM, Wentworth CM (2006) Modeling and Validation of a 3D velocity structure for the Santa Clara Valley, California, for seismic-wave simulations. Bull Seism Soc Am 96:1851–1881. https://doi.org/10.1785/0120050243

Horikawa H, Mizuno K, Ishiyama T, Satake K, Sekiguchi H, Kase Y, Sugiyama Y, Yokota H, Suehiro M, Yokokura T, Iwabuchi Y, Kitada N, Pitarka A (2003) A three-dimensional subsurface structure model beneath the Osaka sedimentary basin, southwest Japan, with fault-related structural discontinuities. Ann Rep Active Fault Paleo Earthq Res 3:225–259 (**in Japanese with English abstract**)

Iwaki A, Iwata T (2011) Estimation of three-dimensional boundary shape of the Osaka sedimentary basin by waveform inversion. Geophys J Int 186:1255–1278. https://doi.org/10.1111/j.1365-246X.2011.05102.x

Iwasaki Y, Kagawa T, Sawada S, Matsuyama N, Oshima K, Ikawa T, Onishi M (1994) Basement structure by airgun reflection survey in Osaka Bay, southwest Japan. J Seism Soc Jpn 46:395–403 (**in Japanese with English abstract**)

Iwata T, Irikura K (1988) Source parameters of the 1983 Japan sea earthquake sequence. J Phys Earth 36:155–184

Iwata T, Kagawa T, Petukhin A, Ohnishi Y (2008) Basin and crustal velocity structure models for the simulation of strong ground motions in the Kinki area, Japan. J Seismol 12:223–234. https://doi.org/10.1007/s10950-007-9086-7

Kagawa T, Sawada S, Iwasaki Y (1992) On the relationship between azimuth dependency of earthquake ground motion and deep basin structure beneath the Osaka plain. J Phys Earth 40:73–83

Kagawa T, Zhao B, Miyakoshi K, Irikura K (2004) Modeling of 3D basin structures for seismic wave simulations based on available information on the target area: case study of the Osaka basin. Bull Seism Soc Am 94:1353–1368. https://doi.org/10.1785/012003165

Koketsu K, Higashi S (1992) Three-dimensional topography of the sediment/basement interface in the Tokyo Metropolitan area, central Japan. Bull Seism Soc Am 82:2328–2349. https://doi.org/10.1785/BSSA0820062328

Koketsu K, Miyake H, Suzuki H (2012) Japan Integrated Velocity Structure Model Version 1, Paper presented at the 15th World Conference on Earthquake Engineering, Lisbon, Portugal, 24–28 September, Paper 1773

Lagarias JC, Reeds JA, Wright MH, Wright PE (1998) Convergence properties of the Nelder-Mead simplex method in low dimensions. SIAM J Optim 9:112–147. https://doi.org/10.1137/S1052623496303470

Lee E-J, Chen P (2016) Improved basin structures in Southern California obtained through Full-3D Seismic Waveform Tomography (F3DT). Seismol Res Lett 87:874–881. https://doi.org/10.1785/0220160013

Lee S-J, Chen H-W, Liu Q, Komatitsch D, Huang B-S, Tromp J (2008) Three-dimensional simulations of seismic-wave propagation in the Taipei basin with realistic topography based upon the spectral-element method. Bull Seism Soc Am 98:253–264. https://doi.org/10.1785/0120070033

Matsushima S, Kawase H (2009) Re-evaluation of strong motion and damage of wooden houses in Kobe city during the 1995 Kobe earthquake. J Struct Eng b. 55B:537–543 (**In Japanese, abstract in English**)

Maufroy E, Chaljub E, Hollender F, Kristek J, Moczo P, Klin P, Priolo E, Iwaki A, Iwata T, Etienne V, De Martin F, Theodoulidis NP, Manakou M, Guyonnet-Benaize C, Pitilakis K, Bard P-Y (2015) Earthquake ground motion in the Mygdonian Basin, Greece: the E2VP verification and validation of 3D numerical simulation up to 4 Hz. Bull Seism Soc Am 105:1398–1418. https://doi.org/10.1785/0120140228

Miyakoshi K, Horike M, Nakamiya R (2013) Long predominant period map and detection of resonant high-rise buildings in the Osaka Basin, Western Japan. Bull Seism Soc Am 103:247–257. https://doi.org/10.1785/0120110334

Moczo P, Kristek J, Galis M, Chaljub E, Etienne V (2011) 3-D finite-difference, finite-element, discontinuous-Galerkin and spectral-element schemes analyzed for their accuracy with respect to P-wave to S-wave speed ratio. Geophys J Int 187:1645–1667. https://doi.org/10.1111/j.1365-246X.2011.05221.x

Nweke CC, Stewart JP, Graves RW, Goulet CA, Brandenberg SG (2022) Validating predicted site response in sedimentary basins from 3D ground motion simulations. Earthq Spectra 38:2135–2161. https://doi.org/10.1177/87552930211073159

Paolucci R, Mazzieri I, Smerzini C (2015) Anatomy of strong ground motion: near-source records and three-dimensional physics-based numerical simulations of the M_w 6.0 2012 May 29 Po Plain earthquake, Italy. Geophys J Int 203:2001–2020. https://doi.org/10.1093/gji/ggv405

Petukhin A, Kagawa T, Koketsu K, Miyake H, Masuda T, Miyakoshi K (2012) Construction and waveform testing of the crustal and basin structure models for southwest Japan. Paper presented at the 15th World Conference on Earthquake Engineering, Lisbon, Portugal, 24–28 September, Paper 2789.

Petukhin A, Sekiguchi H, Kawase H, Kamae K, Tsurugi M (2017a) Large scale simulation of ground motions for heterogeneous source models by FDM reciprocity method. Paper presented at the 16th World Conference on Earthquake Engineering, Santiago Chile, January 9th to 13th 2017, Paper 2932.

Petukhin A, Guo Y, Nishimura T, Tsurugi M (2017b) Site specific probabilistic long-period motions evaluated by FDM reciprocity method. Paper presented at the PSHA Workshop: Future Directions for Probabilistic Seismic Hazard Assessment at a Local, National and Transnational Scale, Lenzburg, Switzerland, September 5–7, 2017, poster C1.

Pitarka A (1999) 3D elastic finite-difference modeling of seismic motion using staggered-grid with non-uniform spacing. Bull Seism Soc Am 89:54–68. https://doi.org/10.1785/BSSA0890010054

Pitarka A, Graves R, Somerville P (2004) Validation of a 3D velocity model of the Puget sound region based on modeling long period ground motion data. Paper presented at the 13th World Conference on Earthquake Engineering, Vancouver, B.C., Canada August 1–6, 2004, Paper 2738.

Sekiguchi H, Asano K, Iwata T, Yoshimi M, Horikawa H, Saomoto H, Hayashida T (2016) Construction of a 3D velocity structure model of Osaka sedimentary basin. Paper presented at the 5th IASPEI / IAEE International Symposium: Effects of Surface Geology on Seismic Motion, Taipei, August 15–17, 2016, Paper P103B.

Suehiro M, Yokokura T, Iwabuchi Y, Kitada N, Pitarka A (2003) A three-dimensional subsurface structure model beneath the Osaka sedimentary basin, southwest Japan, with fault-related structural discontinuities. Ann Report Active Fault Paleoearthquake Res Geol Survey Japan 3:225–259 (**in Japanese with English abstract**)

Takemura S, Akatsu M, Masuda K, Kajikawa K, Yoshimoto K (2015) Long-period ground motions in a laterally inhomogeneous large sedimentary basin: observations and model simulations of long-period surface waves in the northern Kanto Basin, Japan. Earth Planet Space 67:33. https://doi.org/10.1186/s40623-015-0201-7

Wen L, Helmberger DV (1997) Propagational corrections for basin structure: landers earthquake. Bull Seism Soc Am 87:782–787. https://doi.org/10.1785/BSSA0870030782

Yoshida K (2011) Seismic vertical array analysis: Phase decomposition for S and surface waves. Paper presented at the 4th IASPEI/IAEE International Symposium: Effects of Surface Geology on Seismic Motion, University of California Santa-Barbara, August 23–26, 2011.

Publisher's Note